Biol Cybern (2005) 93: 153–170
DOI 10.1007/s00422-005-0559-x

ORIGINAL PAPER

Biological Cybernetics

Chandana Paul · Mario Bellotti · Sašo Jezernik · Armin Curt

Development of a human neuro-musculo-skeletal model for investigation of spinal cord injury

Received: 12 July 2004 / Accepted : 18 March 2005 / Published online: 26 August 2005

Abstract This paper describes a neuro-musculo-skeletal model of the human lower body which has been developed with the aim of studying the effects of spinal cord injury on locomotor abilities. The model represents spinal neural control modules corresponding to central pattern generators, muscle spindle based reflex pathways, golgi tendon organ based pathways and cutaneous reflex pathways, which are coupled to the lower body musculo-skeletal dynamics. As compared to other neuro-musculo-skeletal models which aim to provide a description of the possible mechanisms involved in the production of locomotion, the goal of the model here is to understand the role of the known spinal pathways in locomotion. Thus, while other models focus primarily on functionality at the overall system level, the model here emphasizes functional and topological correspondance with the biological system at the level of the subcomponents representing spinal pathways. Such a model is more suitable for the detailed investigation of clinical questions related to spinal control of locomotion. The model is used here to perform preliminary experiments addressing the following issues: (1) the significance of spinal reflex modalities for walking and (2) the relative criticality of the various reflex modalities. The results of these experiments shed new light on the possible role of the reflex modalities in the regulation of stance and walking speed. The results also demonstrate the use of the model for the generation of hypothesis which could guide clinical experimentation. In the future, such a model may have applications in clinical diagnosis, as it can be used to identify the internal state of the system which provides the closest behavioral fit to a patient's pathological condition.

C. Paul (✉)
Artificial Intelligence Lab, University of Zurich, Andreastr. 15, 8050 Zurich, Switzerland

M. Bellotti · S. Jezernik
Automatic Control Laboratory, ETH Zurich, Physikstr. 3, 8092 Zurich, Switzerland

M. Bellotti · S. Jezernik · A. Curt
Spinal Cord Injury Center, University Clinic Balgrist, Forchstr. 328, 8008 Zurich, Switzerland

1 Introduction

Spinal cord injury can be a debilitating event, often leading to severe loss of locomotor functionality. In some cases, this functionality can be recovered with appropriate clinical care (Rossignol 2000). It has been shown that a form of rehabilitation therapy called treadmill training can improve such recovery (Dietz et al. 1994). However, so far in clinical practice, a uniform training regime has been applied to all patients irrespective of the underlying neural cause of their pathology. As not all injuries lead to the same neural lesions, this is not optimal. The overall recovery of spinal cord injured patients could be greatly improved by identifying the underlying neural cause of a particular pathological condition, and customizing the therapy regime to fit the specific lesion. However, in order to do this, it is first necessary to gain a deeper understanding of the neural mechanisms of the spinal cord involved in locomotion, and the ways in which injury to these mechanisms leads to pathological conditions.

During the last four decades, advances were made in understanding the neural mechanisms involved in the control of locomotion, both with respect to rhythm generation (Shik 1966; Delcomyn 1980; Grillner 1985) and adaptive reflexes (Pearson 1995; Prochazka et al. 2002) in the spinal cord. However, these advances have not yet been integrated into a sufficiently accurate model representing the mechanisms of the spinal locomotor circuits and their functions. Such a neuro-musculo-skeletal model would be a necessary tool to answer questions about neural lesions in the spinal cord, and their effects on locomotor patterns.

Several partial spinal cord models were developed. Some represented mainly the behavior of central pattern generators (Prentice et al. 1998). Others investigated the emergence of locomotion through the interaction of central pattern generators with the musculo-skeletal system (Taga et al. 1991; Taga 1995). In others, more focus was placed on the representation of the reflex pathways and their stabilizing effects on the musculo-skeletal system (Chou 1997). However, these models were not complete.

Recently, development of more complete models of the spinal cord integrated with the musculo-skeletal system was attempted. In the model by Wadden and Ekeberg, reflex pathways were combined with neural phase generators which regulate the reflex gain modulation in each of the four phases of the gait cycle (Wadden and Ekeberg 1998). In another model by Rybak, the half center model of a joint CPG was combined with local Ia, Ib and cutaneous afferent pathways, to produce gait in an accurate musculo-skeletal model of a quadruped hindlimb (Rybak et al. 2002). In a model by Ogihara, central pattern generators were integrated with Ia, Ib and cutaneous pathways, which had interconnections between them whose weights were determined by a genetic algorithm (Ogihara and Yamazaki 2001).

Although these models generated overall behavior resembling locomotor patterns, the topological and functional correspondance to the neural system at the level of the subcomponents was not particularly emphasized. This made them less appropriate for addressing certain types of clinical questions. Firstly, as the subcomponents of the models did not necessarily represent actual neural structures, removal of these components from the system could lead to behavior which was simply an artifact of the model, and not representative of the loss of an actual neural pathways from the biological system. Secondly, as the functional contributions of the reflexes may have been different from the real system, they could bias the prediction of how strongly a particular reflex modality may be required to be active during locomotion. Moreover, differences in functional contributions could lead to the use of components for alternative purposes as compared to the real system. This could lead to inaccurate conclusions about their emergent effects on global behavior. Finally, *lesion studies* in which parts of the network are eliminated in an attempt to match the resultant behavior with a pathological condition, could also provide misleading results. Thus, although these models were useful for providing insights into the high-level control strategies utilized by the neural system for locomotion, they were not designed to address clinical questions regarding the role of known spinal pathways.

For this purpose, a neuro-musculo-skeletal model was required which focused on correspondance to the biological system both at the level of its subcomponents and overall behavior. In addition to the implementation of an accurate musculo-skeletal model, the development of the neural model was deemed to require four stages: implementation of neural subcomponents representing the structure of known spinal pathways, independent tests on each neural subcomponent together with the musculo-skeletal model to ensure functional correspondance, integration of the neural subcomponents into an overall spinal cord model, and further tests on the overall spinal cord model with the musculo-skeletal model to ensure appropriate behavior. The model presented in this paper was the first to be developed according to such a methodology. In the first stage, the subcomponents of the neural model, namely the central pattern generator, Ia, Ib and cutaneous afferent pathways were implemented according to their known topologies from neurophysiology. In the second stage, the 2D musculo-skeletal model, implemented according to the known biomechanical properties of the human body, was used to test each neural subcomponent to ensure appropriate functionality. In the third stage, the neural subcomponents were integrated to produce the overall spinal cord model, and finally this model was tested with the musculo-skeletal model for the ability to generate stable walking behavior.

The model was used to perform experiments to investigate two previously unanswered questions on the role of reflex pathways in walking. The first set of experiments was conducted to study the significance of each of the reflex modalities, and determine whether each reflex modality was necessary for walking. The second set of experiments focused on studying the relative criticality of the reflex modalities, in an attempt to determine which modalities required strong activation during walking and which required only weak activation. The results of these experiments shed new light on these previously unexplored questions and additionally demonstrated the potential of such a model for illuminating the emergent effects of local neural pathways on global system behavior.

The next section, Sect. 2 will outline the topology of the neural spinal cord model (NSCM). Section 3, will then describe the construction of the biomechanical musculo-skeletal model. Section 4 will focus on the first step of validation, that is validation of the individual neural subcomponents. Section 5 will then describe the results of the validation test at the global behavioral level. Section 6 will describe the experiments on the significance and relative criticality of reflex pathways and present the results. Section 7 will discuss the implications of the results and describe the scope for future work, and Sect. 8 will summarize with conclusions.

2 The neuro-musculo-skeletal model

The overall-structure of the neuro-musculo-skeletal model is shown in Fig. 1. The model is comprised of two components, the NSCM, and the musculo-skeletal model. The interaction between these two components is shown by arrows. The following sections will independently describe the neural spinal cord model and the musculo-skeletal model.

2.1 Neural spinal cord model

There is strong evidence suggesting the existence of a spinal central pattern generator in vertebrates which is responsible for rhythmic muscle activation patterns even in the absence of afferent inputs (Shik 1966; Delcomyn 1980; Grillner 1985). Due to evidence suggesting that bipedal walking uses mechanisms involved in quadrupedal locomotion (Dietz 2002a) and measurements of rhythmic movements in spinal cord injured patients, it is also believed that a Central Pattern Generator exists in humans (Calancie et al. 1994). In our NSCM, a central pattern generator module was implemented for each joint, based on the mutually inhibitory half-center model proposed by Brown (1914).

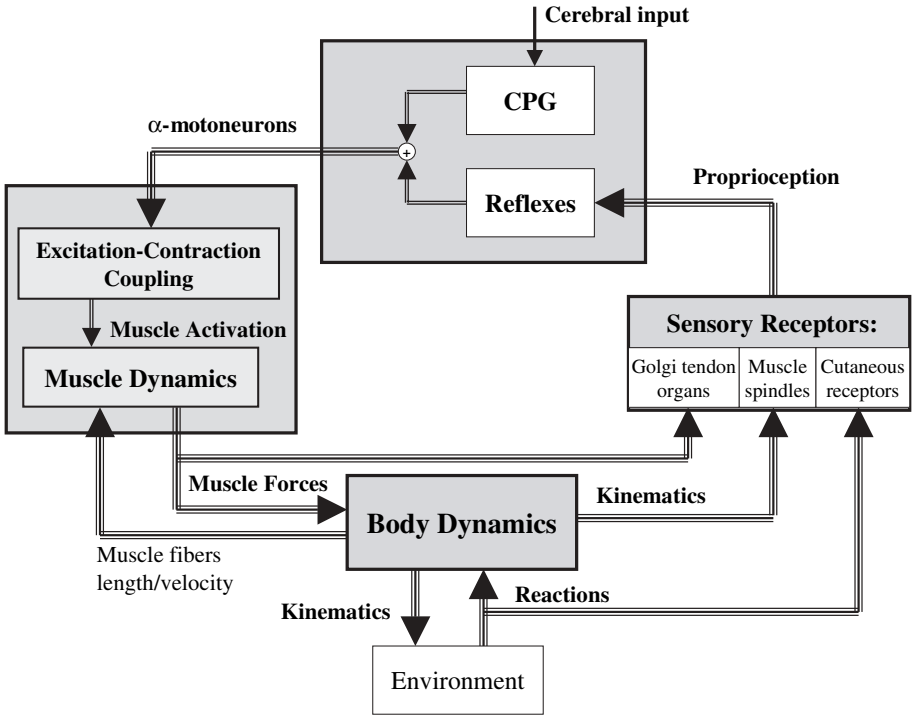

Fig. 1 Diagram indicating the overall structure of the neuro-musculo-skeletal model

Spinal reflexes are known to play an important role in the regulation of locomotion (Schomburg 1988; Pearson 1995). They are involved in shaping the inputs of the centrally generated rhythm (Pearson et al. 1997) and are also modulated during locomotion (Stein and Capaday 1988). Currently the spinal reflexes have been implemented in our model according to the known topology of these pathways as described in (Kandel et al. 1991).

The next sections will describe the different components of the NSCM in detail.

2.1.1 Neurons and sensory receptors

The NSCM was designed as an artificial neural network with recurrent connections. Each neuron received inputs weighted by synaptic weights, and produced an output value according to a piecewise-linear activation function. The equations of the neuron model are given by (1) and (2):

$$\nu_i = \sum_{j=1}^{n} w_{ij} x_j - \theta_i \tag{1}$$

$$\phi(\nu) = \begin{cases} 0, & \nu \leq 0 \\ \nu, & 0 < \nu < 1 \\ 1, & \nu \geq 1, \end{cases} \tag{2}$$

where ν_i is the internal activation of each neuron, x_j are the inputs, w_{ij} are the synaptic weights, θ_i is the threshold or bias and ϕ is the neuron output.

This neuron model was used to implement two kinds of neurons: spinal interneurons and alpha motoneurons. The interneurons usually recieved inputs from afferent neurons or other interneurons and conveyed their output also to other interneurons or alpha motoneurons. The interneurons connected to form various neural modules such as central pattern generators and reflex pathways which finally activated the alpha motoneurons. The alpha motoneurons then activated their corresponding muscle groups.

The neurons which conveyed afferent inputs however, were modeled differently. The muscle spindle receptors had a static and a dynamic component, which correspond to muscle length and muscle velocity, respectively. The static and dynamic gamma motor neurons were not modeled and it was assumed that the response of the primary and secondary endings of the spindle afferents have a constant ratio with respect to the dynamic and static components. Also, it was assumed that the appropriate alpha–gamma coactivation maintains the sensitivity of these receptors at a constant value. The Golgi tendon organ activation was also formed by the contribution of static and dynamic fibers which responded past terms to muscle force and the rate of change of muscle force, respectively. The coefficient of the static fiber was set relatively high as compared to the dynamic coefficient. The contribution of these two fibers were summed to produce the total Golgi tendon organ activation. The cutaneous receptors output a signal which also had two components: one proportional to the ground reaction force and the second proportional to the derivative of the ground reaction force. The general form of receptor activation used can thus be described by the following equations:

$$\mathrm{act}_i(t) = K_p, i \cdot (\mathrm{inp}(t) - \mathrm{inp}_0) + K_d, i \cdot (\mathrm{dinp}(t)/dt) \quad (3)$$

$$K_p = \begin{cases} +a, & \mathrm{inp}(t) \geq 0 \\ -b, & \mathrm{inp}(t) < 0 \end{cases} \quad (4)$$

$$K_d = \begin{cases} +a, & (\mathrm{dinp}(t)/dt) \geq 0 \\ +c, & (\mathrm{dinp}(t)/dt) < 0, \end{cases} \quad (5)$$

where c is zero for muscle spindle receptors and a, b and c are positive constants in the other cases. The $\mathrm{inp}(t)$ is equal to the normalized muscle length, the muscle tendon force, and the ground reaction force for the muscle spindle, Golgi tendon and cutaneous receptor pathways, respectively.

For all three kinds of receptors, the activation is normalized such that the receptor output is a signal which is between 0 and 1. If the lengths or forces become extreme, the sensor activations saturate at a value of 1.

2.1.2 Central pattern generator

The central pattern generator network consists of six neural oscillator units, one for each hip, knee and ankle joint. Figure 2a shows a single oscillator unit. HC Flex and HC Ext are mutually inhibiting half-centers. They are connected to delay circuits, which determine the amount of time each half-center remains active. For the hip and ankle, the extensor and flexor side delay circuits are identical such that each is active for 50% of the cycle. For the knee, the extensor is activated for 67% of the cycle and the flexor for 33% of the cycle. The frequency of oscillation of the neural centers is set to 1 Hz. On the top, there are two input areas which are responsible for initiating the oscillatory dynamics. At the bottom are the motor neurons which receive their activation from the oscillator.

The tonic input of the flexor half-center on the left side is the same as that of the extensor half-center on the right side, and vice versa. This ensures, that at the beginning of walking, the legs begin to move in opposite directions, as is necessary for the generation of a walking pattern.

The joint specific input areas are also responsible for implementing time delays between the different joints, since oscillations of the hip, knee and foot are not synchronous, but phase shifted in time. The six oscillator units are not directly connected with each other, but the timing relationships are maintained by the common tonic input; the hip oscillator is activated first, then the foot with a delay of about 1/10 of a step cycle, and finally the knee with a delay of about 1/5 of a step cycle (Fig. 2b).

2.1.3 Muscle spindle pathways

As described in Sect. 2.1, the muscle spindle receptors have a dynamic and a static component. This is modeled according to the known functional anatomy of the muscle spindle afferents. It has been confirmed that there are two kinds of sensory endings in the muscle spindles. The primary ending consists of the group Ia axons, which are mainly responsible for conveying dynamic information, the rate of change of muscle length. The secondary ending consists of the group II axons which are mainly responsible for conveying static information on muscle length. Both these afferents make monosynaptic excitatory connections to motoneurons innervating the homonymous and synergist muscles of a joint, mediating a stretch reflex (Kandel 1991). Thus, the stretch reflex has both tonic (static) and phasic (dynamic) components. However, the effect of the tonic component is usually significantly lower than the phasic component. Thus, in our model, the stretch reflex has been modeled only as a monosynaptic excitatory pathway from the primary spindle afferent to the alpha motoneuron (Fig. 3a).

The spindle receptors are also responsible for reciprocal innervation, through a spinal interneuron. This reflex is modeled by two pathways: (1) a disynaptic pathway from the group Ia afferents to the alpha motoneuron via an inhibitory interneuron (2) a polysynaptic inhibitory pathway from the group II afferents. (Fig. 3a).

2.1.4 Golgi tendon organ pathways

It was originally thought that the Golgi tendon organ receptors, are connected via a Ib inhibitory interneuron to provide a negative feedback mechanism for regulating muscle stiffness (Kandel 1991). For large values of muscle tension, and in some tasks, this is observed to be the case. However, in locomotion a reflex reversal is observed in which the Ib afferents are used in positive feedback loops (Prochazka et al. 1997a,b). In our network, Ib afferent connections were modeled as two pathways which travel over separate Ib interneurons (Fig. 3a). The threshold of the first Ib interneuron is very high, corresponding to extreme values of muscle tension. This interneuron is connected via an inhibitory connection to the ipsilateral motoneuron of the same muscle. The threshold of the second Ib interneuron is 0, and is connected to the motoneuron via an excitatory connection. Thus, for all low values of muscle tension this pathway is activated. This pathway inhibits itself when the value of muscle tension reaches the threshold of the inhibitory pathway.

2.1.5 Cutaneous pathways

Three types of cutaneous responses have been observed. In the *plantar reflex*, stroking the plantar surface of the foot with a sharp surface from heel to toe leads to a plantar flexion of the toes. In the *extensor thrust reflex*, light pressure on the plantar surface of the foot leads to excitation of the extensor muscles of the same leg. Finally, a painful stimulus to the surface of the foot leads to the *flexion withdrawal reflex* which causes the contraction of all the flexor muscles of the same leg (Kandel et al. 1991).

In our model, the foot was modeled a rigid body so the plantar reflex was not relevant. Furthermore, as the aim was to model walking on level ground with no irregularities to cause painful cutaneous stimuli, the flexion withdrawal reflex was also not applicable. Thus, only the extensor thrust reflex pathways are modeled. The extensor thrust reflex is modeled

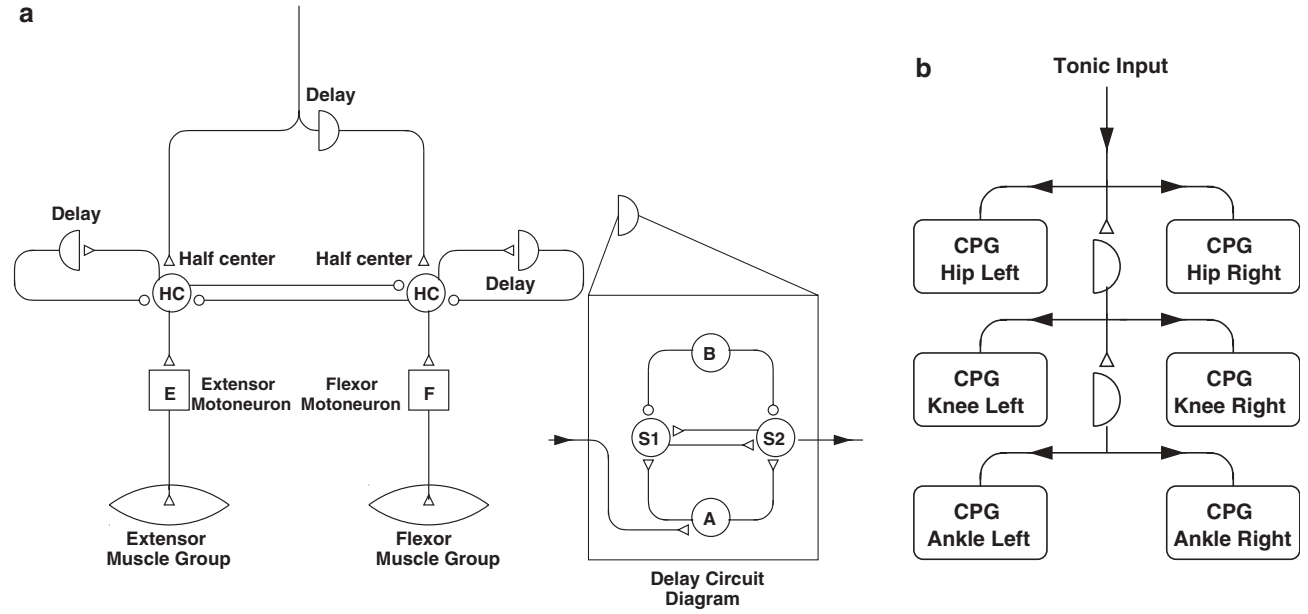

Fig. 2 **a** Central pattern generator circuit for a single joint (△ represents an excitatory connection and ○ represents an inhibitory connection) (**b**) Phase relationships between hip, knee and ankle oscillators (△ represents an excitatory connection and ○ represents an inhibitory connection)

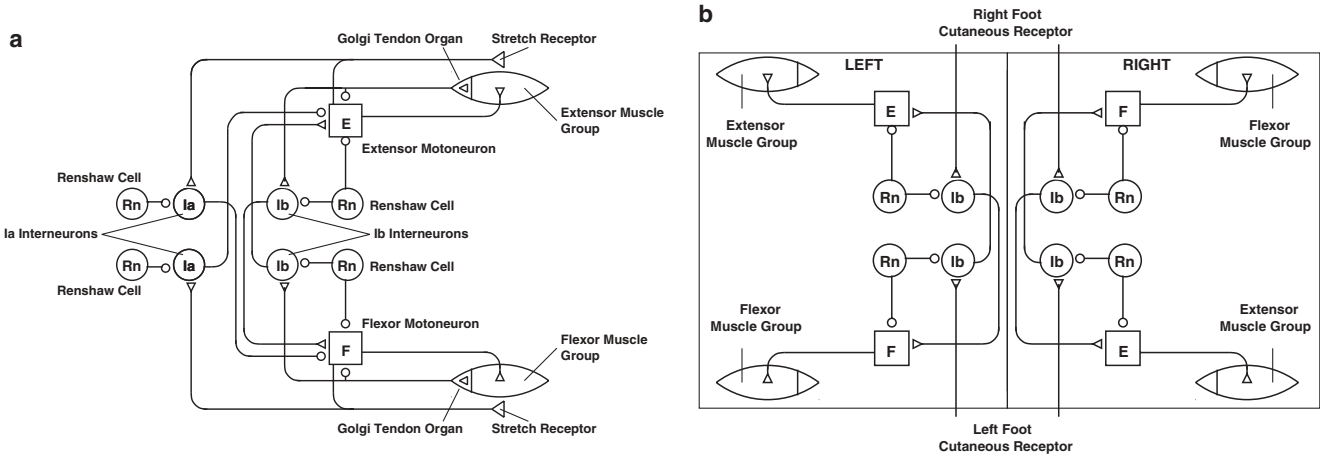

Fig. 3 **a** Spinal reflex pathways corresponding to muscle spindle and Golgi tendon organ receptors (△ represents an excitatory connection and ○ represents an inhibitory connection) **b** Reflex pathways corresponding to right and left cutaneous sensors (△ represents an excitatory connection and ○ represents an inhibitory connection)

as two disynaptic excitatory pathways from the foot cutaneous receptors via Ib interneurons (Fig. 3b). The right cutaneous receptor is connected to a Ib interneuron pathway which excites the extensor muscles of the right leg. It is also connected to a second Ib interneuron which lightly excites the flexor muscles of the left leg.

2.2 Musculo-skeletal model

The biomechanical human body model (BHBM) was developed for the use in combination with the (NSCM) described above. The BHBM is bidirectionally coupled to the NSCM to simulate complex sensory-motor interactions (referring to Fig. 1 the BHBM comprises: excitation-contraction coupling, muscle dynamics, body dynamics and model of environment). A feedforward dynamic simulation of the BHBM, which is fed back to the NSCM, yields the kinematics and kinetics of human locomotion for a given α-motoneuron activation.

2.2.1 Skeletal model

The skeletal model consists of seven segments: the feet, the shanks, the thighs and one segment for the head, arms and trunk (HAT).

The BHBM was implemented in MATLAB using m-scripts and m-functions, and broadly utilizes the MATLAB Symbolic Toolbox. The variables that allow the description of the skeletal system are angles and rotational velocities of the segments, and the displacements and velocities of the upper extremity of the HAT: thus the overall body dynamics has an order of 18 and can be written as

$$D(q) \cdot \ddot{q} + h(q, \dot{q}) = \tau_{\text{muscle}} + \tau_{\text{env}} , \tag{6}$$

where q is the state vector, $D(q)$ is a symmetric, positive definite matrix of inertia, $h(q, \dot{q})$ is a vector representing the Coriolis, centrifugal and gravitational terms, τ_{muscle} represents the torques generated by the muscles, and τ_{env} is a term modeling the interaction with the environment (e.g. the ground reaction forces, the external body unloading system). The positive sign of model variables (joint torques and angles) was defined as shown in Fig. 4. The anthropometric parameters used in the musculo-skeletal model consist of estimates of the geometrical dimensions of different segments and the corresponding kinetic data. These parameters were taken from (Winter 1990) and are summarized in Table 1.

The τ_{muscle} term is calculated by using the muscle model (see Sect. 2.2.2) driven by the motoneuron activations that are input from the NSCM. The τ_{env} term is calculated in the foot-ground reaction model and by considering the Lokomat treadmill conditions (see Sects. 2.2.3 and 2.2.4). The body kinematics q is then obtained by integration of Eq. 6. However, the model relationship given by Eq. 6 also contained an additional knee constraint model. This model provides an angular limit for the knee motion, which prevents the knees from extending beyond the limit $q_{\max}$. The knee constraint

Table 1 Anthropomorphic parameters of the musculo-skeletal model have been set according to Winter (1990)

Part	Mass (kg)	Length (m)	Moment of Inertia
Whole body	80	1.80	
Hat	46	0.85	$M_{HAT} * (0.503 * L_{HAT})^2$
Pelvis	8	0.09	$M_{PELVIS} * (0.8 * L_{PELVIS})^2$
Thigh	8	0.35	$M_{THIGH} * (0.323 * L_{THIGH})^2$
Shank	3.7	0.44	$M_{SHANK} * (0.416 * L_{SHANK})^2$
Foot	1.2	0.07	$M_{FOOT} * (0.475 * L_{FOOT})^2$

model was implemented according to a standard nonlinear constraint model as described by the following equation:

$$\begin{aligned} \tau_{\text{Knee}} &= a_0 \cdot \exp(q_{\text{Knee}} - q_0 + \Delta q_0) \\ &\quad - \sum_{n=0}^{N} a_0 (q_{\text{Knee}} - q_0 + \Delta q_0)^n / n! \\ a_0 &= M_{\max,\text{Knee}} / (\sum_{n=0}^{N} (\Delta q_0)^n / n! - \exp(\Delta q_0)) . \end{aligned} \tag{7}$$

When the joint angle q_{Knee} increases over the limit $q_0 - \Delta q_0$ the moment τ_{Knee} increases monotonically as an exponential derived of the first N+1 terms of the Taylor series. The constant a_0 is calculated based on the value of the moment $M_{\max,\text{Knee}}$ when the angle q_{Knee} reaches its maximum value q_0. The values of the constants were set to: $q_0 = 160$ deg, $\Delta q_0 = 10$ deg, $M_{\max,\text{Knee}} = 100\,\text{Nm}$, $N = 2$.

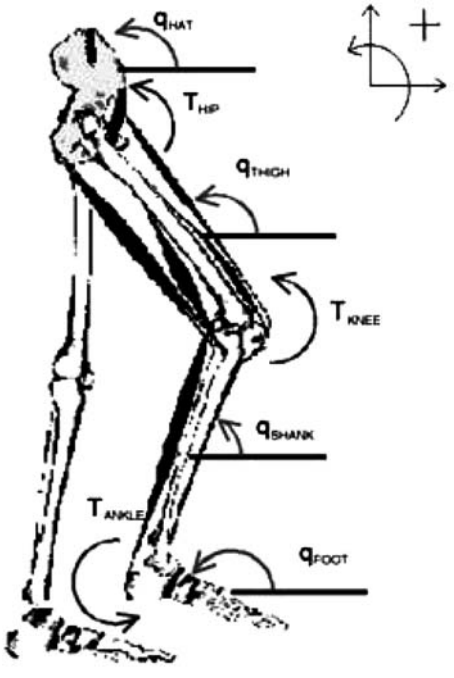

Fig. 4 Definition of the variables of the skeletal model

2.2.2 Muscle model

For every joint, a single muscle representing the whole extensor muscle group and another one representing the whole flexor muscle group were implemented in the model. Since the skeletal model has six joints, and each joint has an extensor/flexor muscle groups, the whole model comprises twelve muscles.

Each muscle was represented by a global muscle model consisting of two parts: the active contractile element and the passive visco-elastic element which act in parallel (McMahon 1984). The active contractile element was modeled by the equation of the standard Hill muscle model (Hill 1938). This equation describes muscle dynamics during voluntary contraction. In the Hill-type models, the active muscle force F_m^{AC} is a product of the muscle activation F_m^{CE}, and the values h_l and h_v which depend on muscle length l_m and muscle velocity l_v, respectively. This is described in the following equation:

$$F_m^{AC} = F_m^{CE} \cdot h_l(l_m) \cdot h_v(v_m) . \tag{8}$$

The functions h_l and h_v implement the force-length and force-velocity relationships experimentally observed in

human muscles. They were modeled as follows:

$$h_l(l_m) = \exp(c \cdot \left| \frac{l_m - l_{m,\text{opt}}}{l_{m,\text{opt}} \cdot w} \right|^3) \tag{9}$$

$$h_v(v_m) = \begin{cases} \frac{v_{m,\max} - v_m}{v_{m,\max} + \varrho \cdot v_m}, & v_m < 0 \\ N_{\text{ecc}} + \frac{v_{m,\max} + v_m}{k \cdot \varrho \cdot v_m - v_{m,\max}}, & v_m \geq 0 \end{cases} \tag{10}$$

The length l_{opt} denotes the optimum length of the contractile element, that corresponds to maximum production of force; the parameter w describes the width of the bell-shaped h_l curve and in our model was set to 1; the value of the constant c is $ln(0.05)$ to fulfill the equation: $h_l(l_{\text{opt}} \cdot (1 \pm w)) = 0.05$.

When a muscle contracts ($v_m < 0$), h_v follows the equation described in (Hill 1938). The parameter $v_{m,\max}$, which has a negative value, specifies the maximum shortening velocity at which the contracting force generation vanishes. k is a shape factor. When a muscle extends ($v_m \geq 0$), h_v follows the equation described in (Aubert 1956). The steepest slope occurs in the neighborhood of $v_m = 0$ and saturates at a high-eccentric velocity, which is the normalized amount of force ($\frac{F_{\text{ecc}}}{F_{\max}}$) reached at the lengthening velocity $v_m = v_{\max}$, (which approximately equals N_{ecc}).

The muscle activation F_m^{CE} is calculated from the motoneuron activation fed to the excitation-contraction coupling model. The relationship between the model input–output is given by Sect. 2.2.2. This equation describes the inverse Laplace transform of alpha motonueron activation filtered by a first-order filter with gain G, zero z and pole p. This linear filter approximates the behavior described by the recruitment and excitation model of (Hatze 2001) and (Zajac 1989). It models the extent of depolarization of muscle cells due to neural stimulation: the stronger the stimulation the larger the region of recruitment. On the other hand, the electrical transmission from the alpha-motoneuron to the muscle fiber is a process that requires a finite amount of time. This was modeled through the effect of the pole p (which corresponds to a time constant $1/p$).

$$F_m^{CE}(A_{\alpha MN(t)}) = L^{-1}\left\{ G \cdot \frac{(1 - s/z)}{(1 - s/p)} \cdot A_{\alpha MN}(s) \right\} \tag{11}$$

The rest lengths of all the muscles were implemented to be identical. The muscles had varying maximum force capacities depending on the muscle group they represented. The maximal muscle forces used are listed in Table 2.

The second component of the muscle model, the passive visco-elastic element acts in parallel to the active contractile element. This component was implemented according to the model of Riener and Edrich (Riener and Edrich 1999) which was experimentally validated on human subjects. The passive component $F_{m,i}^{PA}$ for each muscle is given by the following equation:

$$\begin{aligned} F_{m,i}^{PA} = {} & (\exp(c_1 + c_2 \cdot \phi_{i-1} + c_3 \cdot \phi_i + c_4 \cdot \phi_{i+1}) \\ & - \exp(c_5 + c_6 \cdot \phi_{i-1} + c_7 \cdot \phi_i + c_8 \cdot \phi_{i+1}) \\ & + c_9 + \tau^*_{\text{Knee}})/r_m \end{aligned} \tag{12}$$

Table 2 Maximal muscle forces

Muscle	Max Force (N)
Tibialis Anterior	1000
M. Soleus	500
Vastus Medialis	1000
Biceps Femoris	500
Tensor Fasciae Latae	500
Gluteus Maximus	1000

Table 3 Values of the constants of the passive muscular model as identified for a healthy subject (Riener and Edrich 1999)

Constant	Ankle	Knee	Hip
c_1	2.1016	1.800	1.4655
c_2	–	0.0460	0.0034
c_3	0.0843	0.0352	0.0750
c_4	0.0176	0.0217	–
c_5	−7.9763	−3.971	1.3403
c_6	–	−0.0004	−0.0226
c_7	0.1949	0.0495	0.0305
c_8	0.0008	−0.0128	–
c_9	−1.792	−4.820	8.072

where the subscript i denotes the ankle, the knee or the hip index, and ϕ_{i-1}, ϕ_i and ϕ_{i+1} are the relative angles of the corresponding joints. r_m is the constant moment arm of each muscle, the value of which is set according to (Taga et al. 1991). The values of the constants c_j were identified by Reiner and Edrich through experiments on healthy subjects. These values are listed in Table 3. The component τ^*_{Knee} was added to the equation of the knee only, and equals $e^{(2.220 - 0.150 \cdot \phi_{\text{knee}})}$. This term was added since it allowed a better identification fitting (Riener and Edrich 1999).

For each muscle, the passive torque component τ_m^{PA} is given by $F_{m,i}^{PA} \cdot r_m$ and the active component τ_m^{AC} is given by the product $F_m^{AC} \cdot r_m$ where F_m^{AC} is given by the Eq. 8. The global torque τ_m in Eq. 6 was thus a summation of the active and passive torque components:

$$\tau_m = F_m^{AC} \cdot r_m + F_{m,i}^{PA} \cdot r_m \tag{13}$$

2.2.3 Foot-ground reaction model

As reviewed by Günther in his thesis (Günther 1997), a linear spring-damper constraint is not accurate enough to describe the dynamics of the foot-ground reaction. Therefore, we decided to adopt a nonlinear foot-ground reaction model, which Günther showed to provide best fit to the experimental data.

From a sensitivity analysis of a walking mechanical system, it has been shown that differences in the foot-ground constraint models are the most important causes of differences between simulations and measurements. This is the case because of the impulsive nature of the ground reaction forces which may reach peaks of up to 2000 N within few milliseconds. Thus, we have carefully chosen a foot-ground reaction model for our overall system that provides a good enough

fit for the reaction force data measured during foot-ground contact. Both, the spring and the damping components play an important role to define the actual shape of the reaction force. The best fit model has been adopted from (Günther 1997) to simulate a moving treadmill. It has the following form:

$$\begin{aligned} F_{x,i} &= -E_x \cdot \triangle x_i \cdot |\triangle x_i|^{E_{\text{expx}}} \\ &\quad -G_x \cdot v_{x_i} \cdot |\triangle x_i|^{G_{\text{expx}}} \\ F_{y,i} &= -E_y \cdot \triangle y_i \cdot |\triangle y_i|^{E_{\text{expy}}} \\ &\quad -G_y \cdot v_{y_i} \cdot |\triangle y_i|^{G_{\text{expy}}} \end{aligned} \tag{14}$$

$$\begin{aligned} \triangle x_i &= x_{\text{foot}} - x_{\text{ground}} \\ \triangle y_i &= y_{\text{foot}} - y_{\text{ground}} \\ v_{x_i} &= v_{x_{\text{foot}}} - v_{\text{treadmill}} \\ v_{y_i} &= v_{y_{\text{foot}}} \end{aligned}$$

where i is the foot index (left, right), $F_{x,i}$ and $F_{y,i}$ are the ground reaction force components, $\triangle x_i$ and $\triangle y_i$ are the horizontal and vertical indentations, v_{x_i} and v_{y_i} are the relative foot velocities with respect to the treadmill motion and $v_{\text{treadmill}}$ is the velocity of the treadmill. The equations for $F_{x,i}$ and $F_{y,i}$ represent nonlinear spring and damping reactions with $E_x = 4 \cdot 10^6\,\text{N/m}^2$, $E_y = 1.4 \cdot 10^{12}\,\text{N/m}^{3.5}$, $E_{\text{expx}} = 1$, $E_{\text{expy}} = 2.5$, $G_x = 4 \cdot 10^6\,\text{Ns/m}^3$, $G_y = 2.6 \cdot 10^{12}\,\text{Ns/m}^{4.5}$, $G_{\text{expx}} = 2$, and $G_{\text{expy}} = 3.5$. The vertical indentation $\triangle y_i$ is negative if the foot is below ground level. In the case of no foot-ground contact the force components $F_{j,i}$ are zero. The variable x_{foot} is the local variable with respect to each initiation of foot-ground contact (foot-ground variable x_{ground}). This means that the variable x_{ground} is set anew at each new foot-ground contact event and changes thereafter according to $v_{\text{treadmill}}$. y_{ground} equaled zero.

2.2.4 Lokomat conditions

At the University Hospital Balgrist, the driven gait orthosis Lokomat is used extensively for rehabilitation of spinal cord injured patients (also in the context of this project) (Colombo et al. 2001; Jezernik et al. 2003). The Lokomat system consists of a robotic orthosis with two legs, a harness and a treadmill. The system is used for rehabilitation by inducing walking through actively moving the subjects' legs on a treadmill. The system also allows measurements of gait trajectories, forces, joint torques and ground reaction forces on healthy and impaired subjects. Subjects who have spinal cord lesions and cannot control their leg movements can benefit from this training because the spinal centers below the lesion can be stimulated by induced afferent activity (Dietz 2002). In the first sessions of the treadmill training, the patients are completely passive and the Lokomat completely controls their leg movements. After a few sessions, some voluntary muscle activation can be recovered. During Lokomat therapy, the subject is not required to control upper body posture. the hip is constrained and a harness supports the upper body.

In order to easily compare the simulation data of the NSCM–BHBM model with clinical measurements made in the Lokomat system in healthy and impaired subjects, the Lokomat treadmill conditions were implemented. In our model, body unloading was achieved by adding a vertical force to the center of mass of the trunk, the magnitude of which produced an approximately 60% body unloading. This also generated a torque that helped the upper body remain upright, eliminating the need for postural control. The treadmill condition was implemented as a constant horizontal shift at the foot-ground contact, location that is, in Eq. 15, the velocity $v_{\text{treadmill}}$ was not zero, but had a positive constant value of 0.35 m/s, which resulted in the modification of the term x_{ground}, which now linearly increased with time during the duration of each step.

3 Subcomponent Validation

3.1 CPG tests

In the CPG test, the central pattern generator was validated without the sensory pathways. In this test as an initial condition, the body was vertically suspended, and all the joints were at rest, and free to move. The behavior observed was that the legs began oscillating and after one cycle of motoneuron activation (around 1 s) the movement converged past terms to stable oscillation following a kinematic gait pattern (Fig. 5).

3.2 Muscle spindle tests

In this test, as an initial conditions, the body was suspended and the left thigh was flexed at 90°. All the joints were fixed, except for the left knee. A perturbation was applied such that the knee extensor was stretched for 100 ms until it increased by 20% of its length. After the stretching, the muscle fiber length was set back to the original value due to the geometrical constraint.

The results of the test are shown in Fig. 6. The muscle spindle receptor is not silent before the perturbation, due to the static receptor activity. When the perturbation is applied, a peak is observed in the first part of the perturbation, due to the activation of the dynamic receptor, and it goes rapidly to a steady value, which is higher than the base firing rate (BFR). When the fibers contract after the external stimulation, the sensory activity goes back to BFR. A saturation of MN activation, due to the rapid change of the velocity of the muscle fiber, occurs in the very first part of the perturbation; after it, the MN activity is almost silent. The sharp motorneuron activation leads to a strong torque on the knee joint, corresponding to a sharp contraction of the extensor muscle. This leads to the observed increase in the joint angle, that is, extension of the joint followed by the expected passive flexion of the joint due to gravity. Although the sensory stimulation only lasts for about 50 ms, the extension of the joint angle takes about 300 ms, due to inertia.

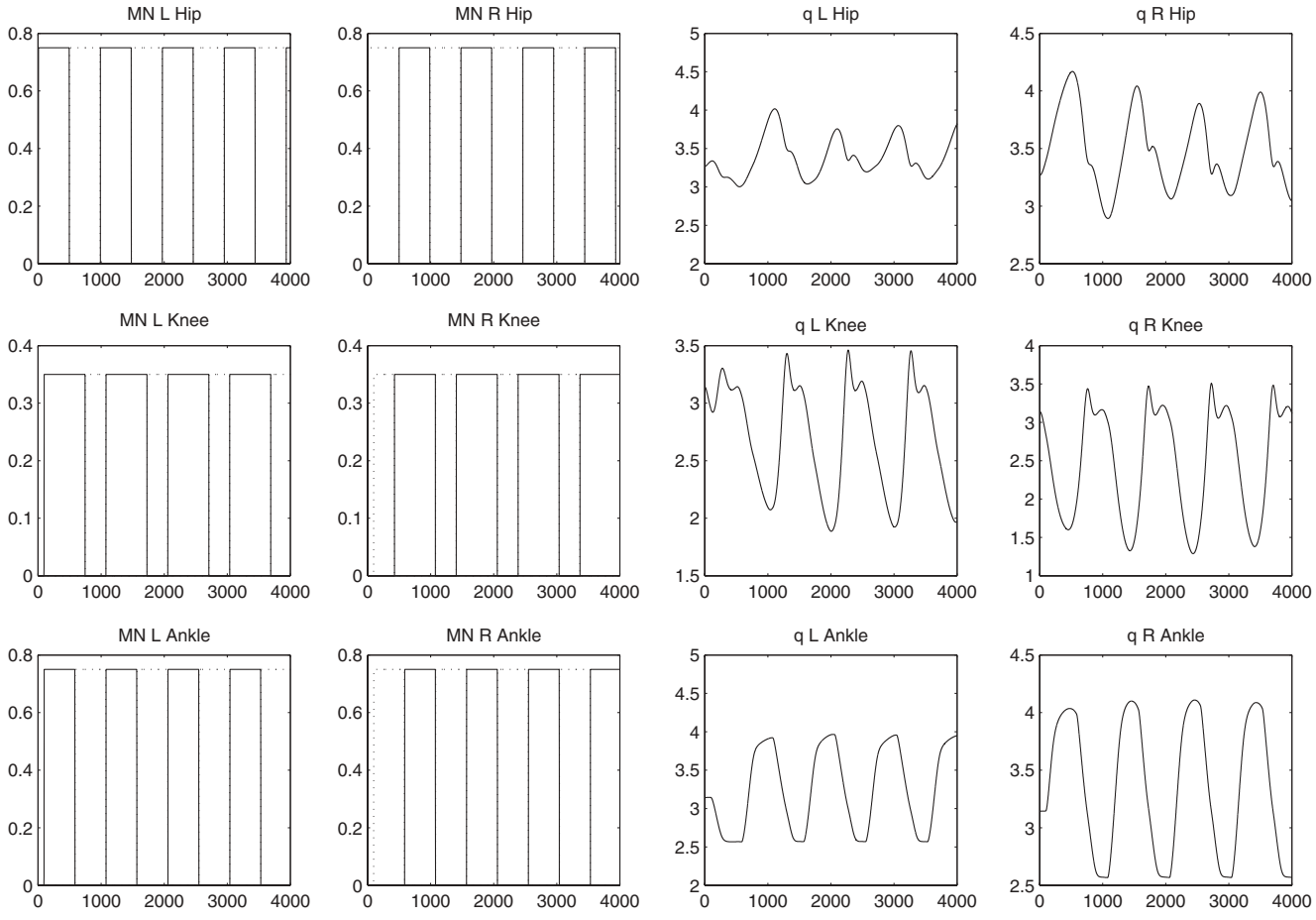

Fig. 5 Results of validation test on the central pattern generator: *a (left)* Motoneuron (MN) activations in the muscles of the hip, knee and ankle joints (The *solid line* represents the extensor and the dotted line, the flexor.) *b (right)* Joint angle displacements (q) of the right and left hip, knee and ankle joints

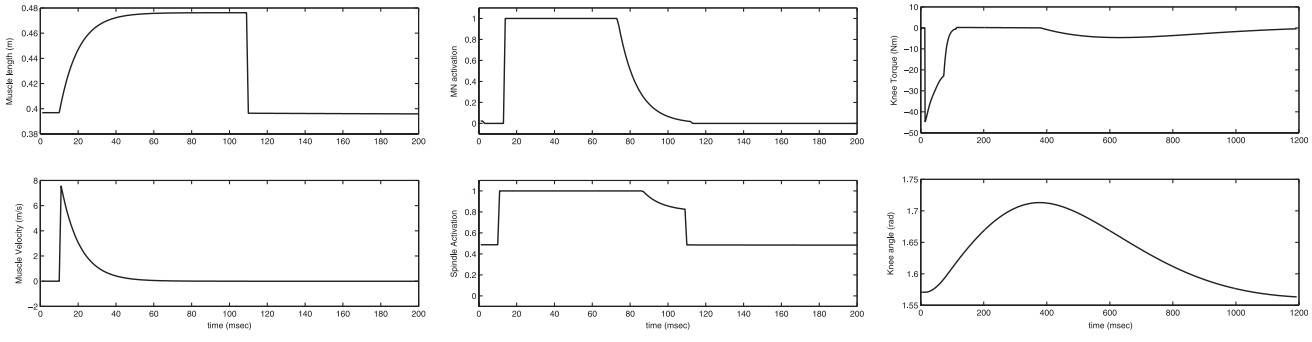

Fig. 6 Results of validation test on the muscle spindle related pathways of the knee joint: **a** muscle length (*top left*) and muscle velocity (*bottom left*) **b** motor neuron activation (*top middle*) and muscle spindle receptor activation (*bottom middle*) **c** joint torque (*top right*) and joint angle (*bottom right*)

3.3 Golgi tendon organ tests

There are two separate Golgi tendon organ based pathways which are differentiated by their functional characteristics as mentioned in Sect. 2.3. The first set of pathways represents the positive force feedback loops which are exhibited during locomotor activity (Prochazka et al. 1997a,b). To validate these pathways, as an initial condition the body was suspended, and the left thigh was flexed at 90°. All the joints, except for the left knee were fixed. The knee extensor and flexor muscles were at rest.

After 100 ms, a mild perturbation of 100 N was applied to the extensor, which was sustained for 500 ms. Due to this perturbation, the Golgi tendon organ receptor responds with an increase in activitiy (Fig. 7). This provokes the reflex, which activates the motor neuron, causing muscle activation. This again results in further Golgi sensor activation, as expected in a positive feedback loop. However, after approximately 300 ms, it can be noticed that the increase in Golgi sensor, motor neuron and muscle activation begin to stabilize, due to the nonlinear properties of the muscle. This is as predicted in experiments with human subjects (Prochazka et al. 1997a).

The second set of pathways represent the negative feedback loops in response to extreme conditions of muscle tension. To validate these pathways, as an initial condition, the body was suspended and the left thigh flexed to 90°; all the joints were fixed, except for the left knee. The knee extensor muscle (Vastus Medialis) was fully activated. A perturbation was applied in which the knee extensor muscle was subjected to a strong force (150% of the maximum force that can be actively generated by the muscle), starting at 100 ms and lasting for 500 ms.

The result of this test are shown in Fig. 8. In the first time step, it is observed that the motoneuron activation goes from 0 to 1. This causes a smooth and delayed muscle activation, due to the ion propagation model. The Golgi receptor senses the increased muscle force and it reaches a value of 0.5. The perturbation starts after 100 ms, when the muscle is fully activated; the Golgi sensor reacts to the strong force applied to the muscle, and fires at maximum rate. This provokes the reflex, which inhibits the motoneuron, causing the delayed decrease in muscle activation, and consequently in the muscle force generated. After approximately 170 ms, the receptor activity is decreased, according to the decrease of muscle force. When the muscle is fully inhibited, the Golgi sensor firing rate reaches the steady state of 0.7. When the force of perturbation is released after 500 ms, the receptor stops firing and thus the reflex is no longer active. This response is as described in (Prochazka et al. 1997a.)

3.4 Cutaneous pathway tests

In the validation test of the cutaneous pathways, as an initial condition, the body is suspended, and all the joints are free. Due to the passive muscular forces, it reaches the equilibrium position with hip and knee slightly flexed and ankle slightly extended. Then, the left cutaneous receptor is stimulated for 50 ms till it reaches the firing rate value of 90% (Fig. 9).

As expected, we observe a strong and rapid activation of the motoneurons of the extensors of the ipsilateral leg, and a weaker and slower activation of the flexors of the contralateral leg. This produces muscle torques that extend all the joints of the left leg and slightly flex all the joints of the right leg. The tests resemble the results shown in (Schieppati and Crenna 1984) in which cutaneous stimulation was observed to produce facilitation of the extensor motoneurons in cats.

4 Overall model behavior

After the individual validation tests of the various modalities were performed as described above, the body was placed on the treadmill and 60% body unloading was achieved by applying an appropriate force at the center of mass of the trunk. All the neural pathways were included into a single model. This gave rise to the issue of determining the appropriate relative strengths of the pathways with respect to each other. At the offset, the relative strength was conceptualized as a "knob" which could influence the gain of a particular category of reflex pathway by a positive multiplicative constant. This knob would alter the amplitude but not the overall function of the reflex pathway. By using four such knobs, k_{CPG}, k_{MS}, k_{GT} and k_{CT}, the relative strengths of the CPGs, muscle spindle pathways, Golgi tendon pathways, and cutaneous pathways could be controlled, respectively. It was decided that the CPG should be fully active during walking, that is, the gain should be 1. Preliminary tests with the gains of the reflex pathways indicated that the model performed well when these gains were lower than the CPG gain, but nonzero. For example, stable walking behavior was acheived on the treadmill when the pathway gains were set to [$k_{CPG} = 1$, $k_{MS} = 0.1$, $k_{GT} = 0.1$, $k_{CT} = 0.3$]. Using these values, the system was able to acheive a stable gait cycle with a walking speed of 0.345 m/s at a rate of 2.2 steps per second. Figure 10 plots the joint angle trajectories for four steps, Fig. 11 plots the joint angle versus angular velocity for 10 s of the walking cycle, and Fig. 12 visually represents the gait cycle over a 2 s time interval.

The results indicate that it is indeed possible to acheive a walking gait cycle by integrating central pattern generators with proprioceptive and cutaneous reflex pathways known from human neurophysiology to be involved in gait generation.

5 Experiments and clinical relevance

While the model is able to successfully generate a walking gait this is not its most significant scientific or clinical contribution. The relevance of such a model lies in the new types of scientific investigations which it enables, as compared to previous models. For example, in previous work, clinical studies were performed investigating cutaneous and proprioceptive

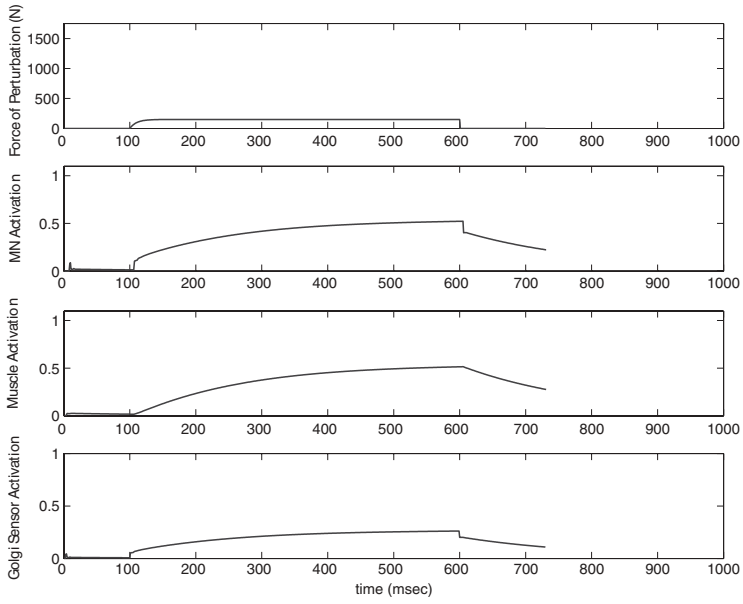

Fig. 7 Results of validation tests on the Golgi tendon organ related positive feedback pathways of the knee extensor: **a** Force of perturbation applied to evoke the reflex response (*top*) **b** motor neuron activation of the muscle (*second from top*) **c** muscle activation (*third from top*), **d** Golgi sensor activation (*bottom*)

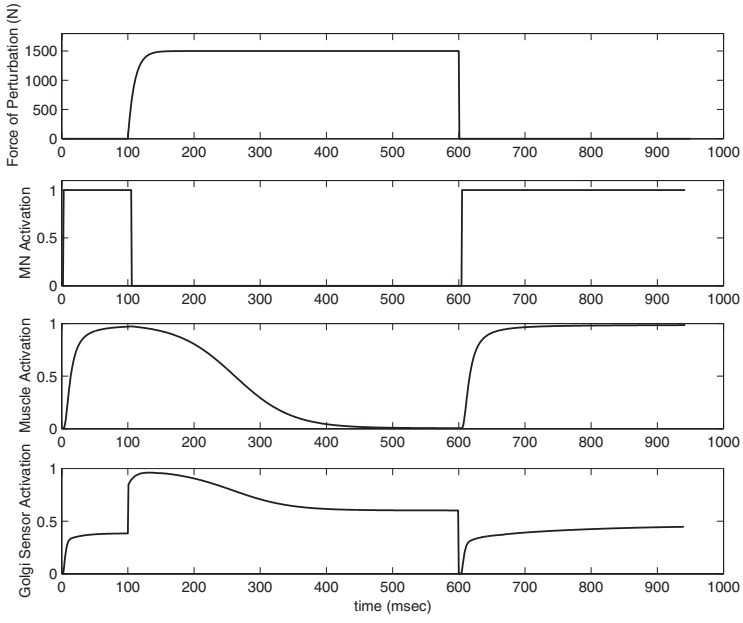

Fig. 8 Results of validation tests on the Golgi tendon organ related pathways of the knee extensor: **a** Force of perturbation applied to evoke the reflex response (*top*), **b** motor neuron activation of the muscle (*second from top*), **c** muscle activation (*third from top*) **d** Golgi sensor activation (*bottom*)

reflexes independently during walking. However, very few could focus on the issue of the relative criticality of the reflexes for walking. It was not known whether the cutaneous reflexes play a larger role than the proprioceptive reflexes or vice versa. It was also not known whether in the realm of proprioceptive sensing, the muscle spindle related pathways were more important than the Golgi tendon organ related reflexes. This information, would be crucial for gaining a deep understanding of the mechanisms controlling walking, not only at the lower levels but at the higher cortical levels as well. For example, if force sensing were much more important than position sensing, we could generate the hypothesis that force-control related representation of motor movements exist in the motor cortex.

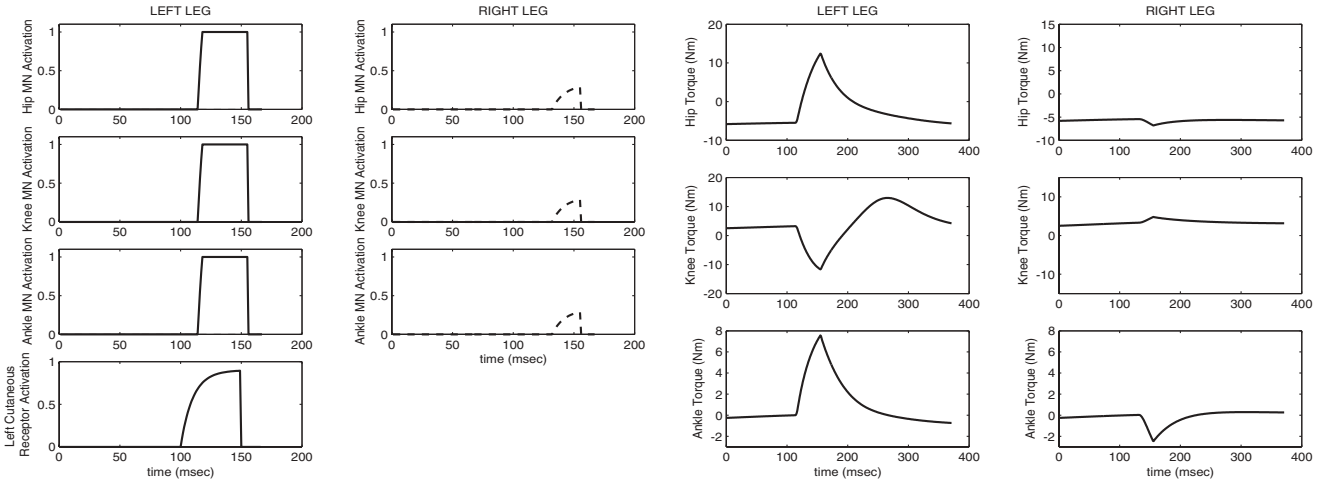

Fig. 9 Results of validation test of the cutaneous pathways, when stimulation is applied to the left foot: **a** activation of extensor muscles of the left leg (*first column from left*) **b** light activation of the flexor muscles of the right leg (*second column*) **c** Joint torques of the left leg (*third column*) **d** Joint torques of the right leg (*fourth column*)

Understanding the relative criticality of the reflex modalities would also prove beneficial in therapy. State-of-the-art therapy for spinal cord injuries involve manual and orthosis-driven treadmill training moving the patients legs through an approximate gait pattern. However if it was known, for example, that one of the reflex pathways was much more important in walking than others, then specific therapies targeting those reflex pathways could be added to the therapy regime.

In contrast to the other investigative techniques, the neuro-musculo-skeletal model described is well suited to the investigation of these issues. The following set of experiments demonstrates the power of this approach, and presents some insightful preliminary results.

5.1 Experiments

In the experiments, the body was always placed on the treadmill, which was moving at a fixed velocity, and suspended by 60%. In the control condition the central pattern generator gain k_{CPG} was set to 1.0, and the muscle spindle pathway gains k_{MS}, golgi tendon organ pathway gains k_{GT} and cutaneous pathway gains k_{CT} were set to 0.1. This condition was selected as it was a condition in which all reflex pathways were equally activated and the model could produce stable walking behavior. This provided a suitable basis for observing changes in gait quality due to variation of system parameters.

The focus of the first study was to investigate the significance of each reflex modality in the system. This was done by recording the effects of deactivation on system behavior. Three experimental conditions were tested as shown in Table 4. In the first experiment, the muscle spindle pathway gains were reduced to 0.0, eliminating the effect of these pathways from the system. In the second experiment, the Golgi tendon organ pathway gains were reduced to 0.0, and in the third, the cutaneous pathways gains. The results of these experiments are given in Table 5. In each case, the performance of the system was drastically reduced from stable walking to stumbling forward and falling. This strongly indicated that each of the reflex modalities played a significant role in the successful performance of the system in the control condition, although the reflex gains were low.

The focus of the second study was to gain insight into the relative criticality of the various reflex modalities. The aim was to record the behavior of the system at low, medium and high values of reflex gain for each modality, where high was defined as being equivalent to the activation of the CPG. Thus, the values 0.1, 0.5 and 0.9 were chosen to sample the range between 0.0 and 1.0. The control case, had the CPG fully active (gain = 1), and all the reflexes set to gain = 0.1. In the first experimental set, the cutaneous pathway gain was altered (gain = 0.5, 0.9), in the second, the Golgi tendon organ pathway, (gain = 0.5, 0.9) and in the third the muscle spindle pathways (gain = 0.5, 0.9). The experimental conditions are summarized in Table 6. If better walking was achieved at a high level of gain than a lower gain, it would indicate that the modality was critical for walking. On the other hand, if the walking was better at a lower gain than at a higher gain, it would indicate that the reflex interfered with walking during certain parts of the gait cycle, and would likely require reflex modulation. Finally, if the walking was unaffected by the level of gain, then it could be concluded that the modality was relatively insignificant for walking.

In each experiment, the body was started from the same initial conditions on a treadmill with the same speed. All other parameters, (excluding the reflex pathway gains) were also equal. An experiment was allowed to continue until the waist height had decreased past a threshold value of 0.45, which was approximately the length of the shank. This indicated that the waist had fallen past the knees, that is, past the point of being able to recover a stable gait. Thus, the duration of the

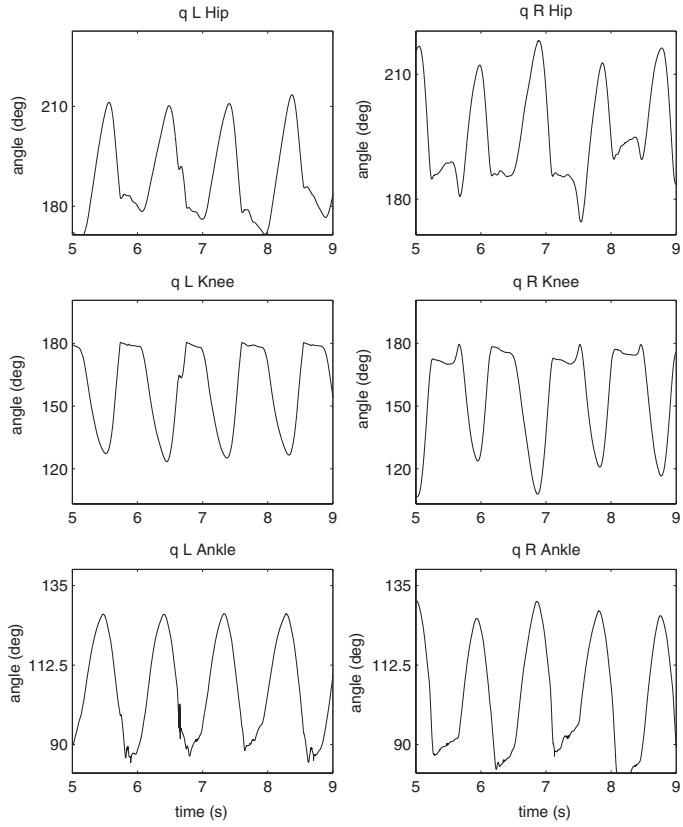

Fig. 10 Joint angle trajectories when the biped has acheived a stable limit cycle, plotted for 4 s. The abscissa shows time in milliseconds, and the ordinate shows the joint angle in degrees

experiment was directly correlated to the quality of the gait, and could be used as metric for comparison. In addition to the quantitative data, qualitative information about the quality of the gait cycle was also relevant. Both these quantitative and qualitative results of the experiments are presented in Table 7.

In the control condition, stable stepping was acheived but the velocity was low (Fig. 13). In the first set of experiments where the muscle spindle gain was altered, it was observed that at both mid-range and high values of gain, the walking was strongly impaired; the biped was able to take only 5–6 steps before falling forward. A major contribution to the fall was the buckling of the knees during stance phase as can be seen in Fig. 14. It appeared as though the flexors of the knees which were stretched during stance phase, produced too strong an opposing contraction, causing the knee to flex and buckle during the stance.

In the second set of experiments, the results were interesting. At both mid-range and high values of gain, it was found that within the range of gains chosen, no significant difference was produced in the gait pattern compared to the control condition (Fig. 15). The data does not necessarily suggest that force dependent reflexes do not play a significant role during walking. However, they do suggest that within a certain range, positive force feedback does not decrease the stability of the system, as suggested by results from Prochazka.

Table 4 Experimental conditions in deactivation study: In condition 1 the muscle spindle related reflex pathways are deactivated by setting the gain to 0, in condition 2 the Golgi tendon organ related pathways are similarly deactivated, and in condition 3 the cutaneous reflex pathways gains

	k_{CPG}	k_{MS}	k_{GT}	k_{CT}
1	1	0.0	0.1	0.1
2	1	0.1	0.0	0.1
3	1	0.1	0.1	0.0

In the third set of experiments, in which the cutaneous pathway gains were altered, it was found that although the stability of the gait was affected for the worse, the quality of the gait improved (Fig. 16). In the control condition, stable stepping was observed, but since the step length was quite small, the gait almost resembled stepping in place, causing the body to move backwards along with the treadmill. With an increased value of cutaneous reflex pathway gain, the gait matched the speed of the treadmill more closely and was able to take on the order of 10–20 steps before starting to walk forward and fall over. In the case of the mid-range gain,

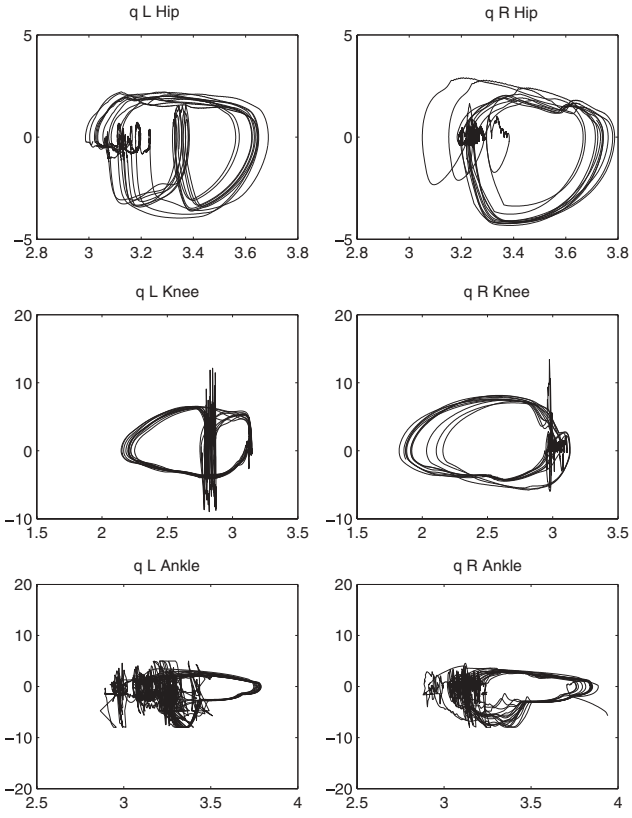

Fig. 11 Phase plots of joint angle versus angular velocity, plotted for 10 s

Table 5 Results of deactivation studies

MS	GT	CT	**Duration** (s)	**Steps**	**Speed** (m/s)	**Behavior**
0.0	0.1	0.1	3.6	5	0.05	almost unable to step, falls forwards
0.1	0.0	0.1	3.9	6	0.08	almost unable to step, falls forwards
0.1	0.1	0.0	6.6	5	−0.10	almost unable to step, falls forwards

the speed acheived was 0.44 m/s, and in the case of the high gain the speed acheived was 0.54 m/s. Thus, also considering the results of the overall test, where a cutaneous pathway gain of $k_{CT} = 0.3$ produced a walking speed of 0.345 m/s, it was possible to observe a monotically increasing relationship between the cutaneous pathway gain and walking speed.

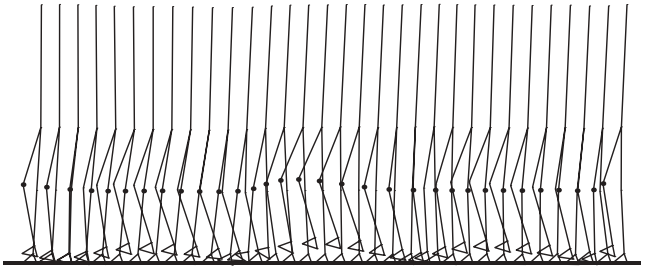

Fig. 12 Gait pattern after the biped has reached a stable limit cycle, shown for 2 s

6 Discussion

The results of the experiments provide interesting preliminary insights into the relative criticality of the different reflex pathways. It seems that the muscle spindle based stretch reflexes must remain at a low value of gain during walking, in order to enable stepping. The gain of the Golgi tendon organ based reflexes do not seem very critical within a certain range. The cutaneous reflex gain on the other hand is observed to be correlated to the speed of walking.

Further work both in simulation as well as with human subjects, will be required to more strongly qualify these results. Currently, the model uses a pure feed-forward CPG model which does not change frequency based on sensory feedback. Taga showed that an adaptive CPG greatly increases the basin of stability of the system (Taga 1991) and is likely to be the case in biology. In the experiments here, however, the results may not change greatly due to an adaptive CPG. In the case where the Muscle Spindle based reflex

Table 6 Experimental conditions in gain modulation study: In Set 1 muscle spindle related reflex pathway gains are altered, in Set 2 the Golgi tendon organ related pathway gains, and in Set 3 the cutaneous reflex pathway gains. The line in bold indicates the control condition, which is identical over all sets

	k_{CPG}	k_{MS}	k_{GT}	k_{CT}
	1	**0.1**	**0.1**	**0.1**
Set 1	1	0.5	0.1	0.1
	1	0.9	0.1	0.1
	1	**0.1**	**0.1**	**0.1**
Set 2	1	0.1	0.5	0.1
	1	0.1	0.9	0.1
	1	**0.1**	**0.1**	**0.1**
Set 3	1	0.1	0.1	0.5
	1	0.1	0.1	0.9

pathway gains are increased, the problem will always remain that the extensors of the knee joints are turned off in stance phase. Thus, buckling will cause an instability whether or not the CPG receives sensory feedback. The Golgi tendon organ pathways do not significantly effect the stability of the system, and this would not change if the CPG were to receive sensory feedback. As far as the cutaneous pathways are concerned, it seems that the cutaneous reflex increases the stride length by additional activation to the hip muscles. This effect would continue to exist in a system with an adaptive CPG, although the stability may not deteriorate as much as seen in the experiments. Thus, the accuracy of the model could be improved by including adaptivity in the CPG.

The model could also be improved by the inclusion of bi-articular muscles. Although, the bi-articular muscles are redundant in function, and thus the results of reflex conditions on these muscles have similar effects to those observed, the accuracy of the model would nonetheless improve by inclusion of these muscles. The model could also be improved in accuracy by the inclusion of series elasticity in the muscles, neural latencies, and interjoint connections in Ib interneurons. In a future step, it would also be worthwhile to extend the model to 3D.

Nonetheless, the experiments performed here serve to the highlight the potential of such a neuro-musculo-skeletal model for the investigation of clinical issues. In addition to further sampling the space of reflex pathway gains by modality as performed above, various other studies can be undertaken. Studies can be performed of the relative strength of reflex gains by joint. It is likely that some reflexes are more strongly activated in some joints than in others, depending on their utility during the gait cycle. By sampling the space of relative reflex gains by joint, using an optimization algorithm, the relative gains which lead to successful gait could be determined. The model could also be used to address the more complex issue of temporal reflex gain modulation, using a similar approach.

Another area of interest, which has been difficult to address using other techniques is that of reflex pathway interconnectivity. It is known that in the case of the proprioceptive reflex pathways, a sensory stimulus from one muscle not only activates the reflex in the homonymous muscle but also other muscles which may or may not be in the same muscle group. The topology of these interconnections is not entirely clear. Using the model however, it would be possible to assess the effect of an interconnection on the resulting quality of gait, and therefore determine likely interconnection schemes.

Another important issue that can be addressed using the model is the relationship between the CPG and the reflexes. On one hand simple questions regarding the relative gains of the CPG versus the reflexes can be addressed, using a similar approach to the experiments above. However, more complex issues such as the interconnections between the reflexes and the CPG can also be addressed. For example, it is known that the cutaneous reflex pathway is responsible for resetting the central pattern generator from swing phase to stance phase. On the other hand, the joint proprioceptors are responsible for sensing the end of stance phase, and for initiating the swing phase. These interdependencies can easily be investigated in the model by introducing the hypothesized connections between the proposed reflex pathways and the CPG.

Very few models have focused on two or more reflex modalities simultaneously and their inter-relationships during the walking cycle. Thus, the function of these reflex pathways are understood only in isolation, with respect to the other parts of the system. This leads to a bias in current literature toward attributing a direct gait related function to each reflex. However, studies of behavior-based systems have shown that in a system of multiple reflexes, some reflexes may serve to simply create the right conditions to activate other, more significant, reflexes. Therefore the function of a

Table 7 Results of gain modulation studies

MS	GT	CT	**Duration** (s)	**Steps**	**Speed** (m/s)	**Behavior**
0.1	0.1	0.1	50.0	48	0.08	Stable stepping, very low velocity
0.5	0.1	0.1	3.1	3.5	0.24	Almost unable to step, falls forwards
0.9	0.1	0.1	3.9	3	0.14	Almost unable to step, falls forwards
0.1	0.1	0.1	50.0	48	0.08	Stable stepping, very low velocity
0.1	0.5	0.1	50.0	53	0.10	Stable stepping, very low velocity
0.1	0.9	0.1	38.1	41	0.19	Stable stepping, low velocity
0.1	0.1	0.1	50.0	48	0.08	Stable stepping, very low velocity
0.1	0.1	0.5	9.6	11	0.44	Walking forward, falling after several steps
0.1	0.1	0.9	9.1	10	0.54	Walking forward, falling after several steps

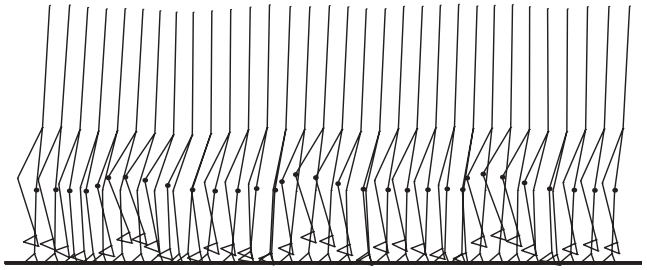

Fig. 13 Movement pattern achieved in the control condition [$k_{MS} = 0.1$, $k_{GT} = 0.1$, $k_{CT} = 0.1$], plotted once every 100 ms. Each stick figure is plotted at a constant distance interval from the previous time step.

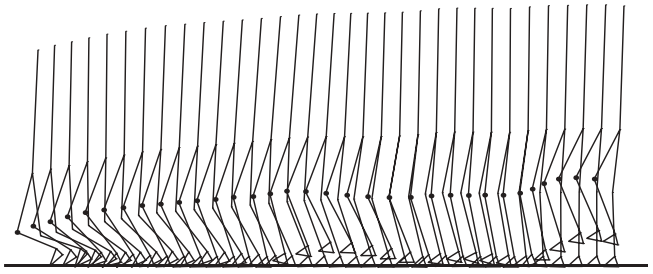

Fig. 14 Movement pattern acheived in the case [$k_{MS} = 0.5, k_{GT} = 0.1$, $k_{CT} = 0.1$], plotted once every 50 ms. Each stick figure is plotted at a constant distance interval from the previous time step.

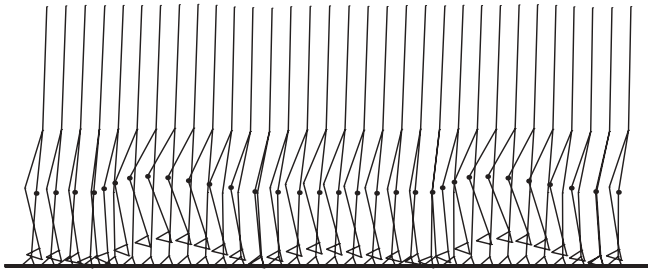

Fig. 15 Movement pattern acheived in the case [$k_{MS} = 0.1, k_{GT} = 0.5$, $k_{CT} = 0.1$], plotted once every 50 ms. Each stick figure is plotted at a constant distance interval from the previous time step.

reflex may not directly relate to a key transition in the gait cycle, but may induce a small change which then triggers another reflex causing a key transition. This complexity has been largely ignored in the biological literature to date. The possibility to address these questions makes a model developed using subcomponent and system validation versatile in its range of potential applications.

6.1 Topological versus functional modeling

The main difference between the methodology used in this work, compared to previous work, is that we have used a largely *topological modeling* strategy as opposed to a

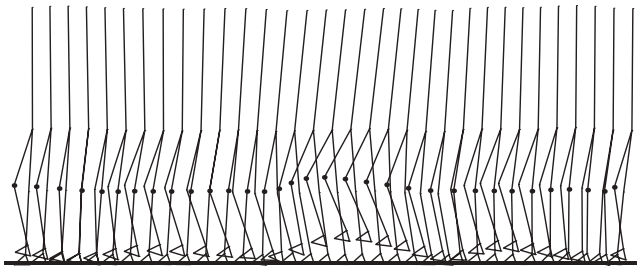

Fig. 16 Movement pattern achieved in the case [$k_{MS} = 0.1, k_{GT} = 0.1$, $k_{CT} = 0.5$] plotted once every 50 ms. Each stick figure is plotted at a constant distance interval from the previous time step.

functional modeling approach. In a functional modeling approach, the function of a certain neural module is first modeled as an abstract mathematical function or artificial neural network whose structure is an abstraction from the actual architecture of the neural pathways in biology. The quality of such a model is judged by comparing its functional performance to the known function of the neural module. If the model replicates the overall behavior of the system sufficiently well, it can be said that the model represents a viable hypothesis about the mechanisms involved in the system. In a topological modeling approach however, the aim is not to suggest a hypothesis about the mechanisms involved in the system, but to understand how known neural pathways contribute to the overall functioning of the system. Thus, a neural module is implemented according to its known topology, and evaluated by comparing its functional performance against its known immediate function. By putting this together with other pathways, and observing the emergent pattern of behaviors, the more indirect contributions of the module in the context of the complex system can be assessed.

Each modeling approach has its own advantages and disadvantages, and is more or less suited to a particular type of scientific enquiry. The functional modeling approach has the advantage that it can lead to simple models, with explanatory power over a complex system. The disadvantage is that there can be several functional models which can produce the same overall behavior, and it is difficult to decide which one most accurately represents the real system. A functional model is most suitable for understanding systems in which the overall behavior is easy to measure, but the neural pathways have not been well described, or a system in which the pathways have been well described but an abstract level of understanding about the system is necessary.

The topological modeling approach on the other hand, is appropriate when the topology of a module is well known, but where all the functional contributions of that module may not be fully understood. There are, of course, certain disadvantages of the topological modeling approach as well. Firstly, using the topological approach for the modeling of a complex system can be cumbersome. The number of neural units and parameters can quickly escalate into the thousands, making the system large and slow. The model as it stands now, for example, already has over 300 nodes and 600 synaptic connections. Secondly, in topological modeling there is always the question "Is there enough detail?" For example,

it can be argued that a more detailed neural model should be used, which includes temporal characteristics such as spiking. The problem is that it is difficult to assess when the level of accuracy is appropriate. The only way to do this would be to include the feature under debate, and note whether it effects a significant change in the behavioral output of the system. If the change is large, then the feature is important for the model. Unfortunately, this is a cumbersome task to undertake for every feature that can possibly be included in the system. Finally, topological modeling is limited by the current knowledge of neural pathways in biology. Only neural modules whose topology is relatively well known can be included in a topological model. Thus, it can be argued that topological modeling cannot provide any new insights, in addition to what is already known in biology.

However, as shown above, there is some utility of a topological model as compared to a functional model. Although the topology of a particular neural pathway may be known, along with perhaps its direct function, its multiple range of functions in the system may not be known. By putting together known pathways, and seeing how they interact to produce a particular behavior, the functional contributions of that module may be more deeply understood. For example, it has been previously known that cutaneous pathways are crucial for the control of stance phase, but it was not known that the pathway may be involved in the regulation of walking speed. In this way, even a topological model with limited accuracy can generate new insights into the functional contributions of existing structures.

6.2 Clinical application

In addition to these theoretical contributions, the model also has applications in clinical practice for the rehabilitation of spinal cord injured patients. Incomplete spinal cord injury, involving a partial lesion of the neural pathways of the spinal cord, can lead to various locomotor deficits depending on the location and size of the lesion. However, for a clinician with access to only the external pathologies of the patient, it is difficult to determine the exact nature of the internal lesion, and thus to prescribe an optimal therapy regime. Use of the neuro-musculo-skeletal model can help greatly in this respect. A host of different lesions can be performed on the model, and the resultant gait pattern can be recorded in a database. Then when a patient's gait pattern is recorded, statistical methods can be used to determine the pattern of lesions which has the closest fit to the patient's condition. A more advanced method can be to develop a "reverse engineering" algorithm for use with the model, which enables the settings of gain and lesion parameters to be determined for any arbitrary gait pattern, providing invaluable diagnostic information to the clinician.

7 Conclusion

This paper describes the design and implementation of a biomimetic human neuro-muskulo-skeletal model, which is composed of a NSCM with high topological accuracy, and a biomechanical human body model. The NSCM contains neural modules corresponding to central pattern generators and muscle spindle, Golgi tendon organ and cutaneous sensor based reflex pathways. Each of the subcomponents of the model are independently validated before inclusion into the overall model, and the system is shown to produce stable walking. The scientific potential of such a topological model is demonstrated in the experiments related to relative criticality of reflex pathways. The results provide interesting insights into the importance and function of the various reflex pathways in walking.

Acknowledgement This research was supported by the Swiss National Science Foundation (SNF) project 3152-062025.00/1 "Improving Locomotor Functions in Spinal Cord Injured Patients." The authors would also like to acknowledge the contributions of Manfred Morari, Hansrvedi Frueh, Rolf Pfeifer and Volker Dietz.

References

Aubert X (1956) Le couplage de la contraction musculaire. Edition Arscia Brussels, Thesis

Brown TG (1914) On the nature of the fundamental activity of the nervous centers; together with an analysis of the conditioning of rhythmic activity in progression, and a theory of the evolution of function in the nervous system. J Physiol Lond 48:18-46

Calancie B, Needham-Shropshire B, Jacobs P, Willer K, Zych G, Green BA (1994) Involuntary stepping after chronic spinal cord injury. Evidence for a central rhythm generator for locomotion in man. Brain 117(5):1143–1159

Chou CP, Hannaford H (1997) Study of human forearm posture maintenance with a physiologically based robotic arm and spinal level neural controller. Biol Cybern 76:285–298

Colombo G, Joerg M, Schreier R, Dietz V (2001) Treadmill training of paraplegic patients with a robotic orthosis. J Rehabil Res Dev 37:693–700

Delcomyn F (1980) Neural basis of rhythmic behavior in animals. Science 210(4469):492–498

Dietz V, Colombo G, Jensen L (1994) Locomotor activity in spinal man. Lancet 344:1260

Dietz V (2002a) Do human bipeds use quadrupedal coordination? Trends Neurosci 25(9):462–467

Dietz V, Mueller R, Colombo G (2002b) Locomotor activity in spinal man: significance of afferent input from joint and load receptors. Brain 125:2626–2634

Grillner S (1985) Neurological Bases of Rhythmic Motor Acts in Vertebrates. Science 228:143

Günther M (1997) Computersimulationen zur Synthetisierung des muskulär erzeugten menschlichen Gehens unter Verwendung eines biomechanischen Mehrkf̂7rpermodells, Dissertation of the University of Tubingen

Hatze H (2001) An efficient simulation method for discrete-value controlled large scale neuromyoskeletal system models. J Biomech 34:267–271

Hill AV (1938) The heat of shortening and the dynamic constants of Muscle. Proc Roy Soc 126(B):136–195

Jezernik S, Colombo G, Keller T, Frueh H, Morari M (2003) Robotic Orthosis Lokomat: A Rehabilitation and Research Tool. Neuromodulation 6(2):108–115

Kandel ER, Schwartz JH, Jessell TM (1991) Principles of neural science. Elsevier Science Publishing Co., New York

McMahon TA (1984) Muscles, reflexes, and locomotion. Princeton University Press, Princeton

Ogihara N and Yamazaki N (2001) Generation of human bipedal locomotion by a bio-mimetic neuro-musculo-skeletal model. Biol Cybern 84:1–11

Pearson KG (1995) Proprioceptive regulation of locomotion. Curr Opin Neurobiol 5:786–791

Pearson KG, Ramirez JM (1997) Sensory modulation of pattern generating circuits. In: Stein PSG, Grillner S, Selverston A, Stuart DG (eds) Neurons, networks and motor behavior MIT Press, Cambridge, pp 225–236

Prentice SD, Patla AE, Stacey DA (1998) Simple artificial neural network models can generate basic muscle activity patterns for human locomotion at different speeds. Exp Brain Res 123:474–480

Pratt CA (1995) Evidence of positive force feedback among hindlimb extensors in the intact standing cat. J Neurophysiol 73(6):2578-83

Prochazka A, Gillard D, Bennett DJ (1997a) Positive force feedback control of muscles. J Neurophysiol 77(6):3226–3236

Prochazka A, Gillard D, Bennett DJ (1997b) Implications of positive feedback in the control of movement. J Neurophysiol 77(6):3237–3251

Prochazka A, Gritsenko V, Yakovenko S (2002) Sensory control of locomotion: reflexes versus higher-level control. In: Gandevia SG, Proske U, Stuart DG (eds) Sensorimotor control. Kluwer London

Riener R, Edrich T (1999) Identification of passive elastic joint moments in the lower extremities. J Biomech 32:539–544

Rossignol S (2000) Locomotion and its recovery after spinal injury. Curr Opin Neurobiol 10(6):708–716

Rybak IA, Ivashko DG, Prilutsky BI, Lewis MA, Chapin JK (2002) Modeling Neural Control of Locomotion: Integration of Reflex Circuits with CPG. In: Proceedings of international conference on artificial neural networks 2002, pp 99–104

Schieppati M, Crenna P (1984) Natural cutaneous stimulation induces late and long-lasting facilitation of extensor motoneurons in the cat. Brain Res 293(2):259–267

Schomburg ED, Petersen N, Barajon I, Hultborn H (1998) Flexor reflex afferents reset the step cycle during fictive locomotion in the cat Exp Brain Res 122:339–350

Shik ML, Severin FV, Orlovskii GN (1966) Control of walking and running by means of electric stimulation of the midbrain. Biofyzika 11:659

Stein RB, Capaday C (1988) The modulation of human reflexes during functional motor tasks. Trends Neurosci 11:328–332

Taga G, Yamaguchi Y, Shimizu H (1991) Self-organized control of bipedal locomotion by neural oscillators in unpredictable environment. Biol Cybern 65:147–159

Taga G (1995) A model of the neuro-musculo-skeletal system for human locomotion. Biol Cybern 73:97–111

Wadden T, Ekeberg O (1998) A neuro-mechanical model of legged locomotion: single leg control In: Biol Cybern 79:161–173

Winter D (1990) Biomechanics and motor control of human movement, 2nd edn. Wiley, New York

Zajac FE (1989) Muscle and Tendon: properties, models, scaling and applications to biomechanics and motor control. CRC Crit Rev Biomed Eng 17:359–419